

A note on the amplitude modulation phenomenon in non-canonical wall-bounded flows

Mitchell Lozier,* Ivan Marusic, and Rahul Deshpande

Department of Mechanical Engineering, The University of Melbourne, Victoria 3010, Australia

(Dated: September 4, 2024)

The amplitude modulation phenomena, defined originally by Mathis *et al.* (J. Fluid Mech., **628**, 311-337; 2009), corresponds to a unique non-linear interaction between Reynolds number (Re_τ) dependent large-scale motions and Re_τ -invariant inner-scale motions observed in canonical wall-bounded flows. While similar non-linear interactions can be observed in non-canonical wall-bounded flows, linking them to amplitude modulation is questionable due to the fact that each non-canonical effect is associated with distinct variations in the energies of both the large and inner scaled motions. This study investigates non-linear triadic interactions as a function of various non-canonical effects by analyzing published hot-wire datasets acquired in the large Melbourne wind tunnel. It is found that triadic interactions, across the entire turbulence scale hierarchy, become statistically significant with increasing intensity of non-canonical effects such as rough walls, pressure gradients, and spanwise or wall-normal forcing. This stands in contrast to previous observations made in canonical flows, where only the interaction between inner scales and inertia-dominated large scales was considered dynamically significant for increasing Re_τ . The implications of these findings are discussed for near-wall flow prediction models in non-canonical flows, which must take into account all coexisting non-linear triadic interactions in wall-bounded flows.

I. INTRODUCTION AND MOTIVATION

A characteristic feature of all turbulent flows is a broad range of turbulent scales of motion, which are non-linearly coupled across the energy spectrum. This inter-scale coupling/interaction regulates the energy transfer mechanisms that drive several technologically relevant flows, such as the turbulent boundary layer (TBL). TBLs encountered in engineering applications are typically exposed to non-canonical effects/perturbations, such as wall roughness, pressure gradients, etc., which affect these inter-scale interactions in a non-trivial manner. Here we will discuss a well-known inter-scale interaction, *i.e.* the amplitude modulation phenomenon [1, 2], in the context of non-canonical wall-bounded flows. Before investigating non-canonical effects, however, we will first define the various terminologies and revisit the established knowledge on inter-scale interactions in a canonical TBL, *i.e.* a zero-pressure gradient (ZPG) TBL over a hydraulically-smooth wall.

Figure 1 depicts a spectral representation of the energy distribution across a broad hierarchy of scales coexisting in a high-Reynolds number ($Re_\tau > \mathcal{O}(10^3)$) canonical TBL [3]. It is presented as the premultiplied frequency (f) spectra of the streamwise velocity fluctuations ($f\phi_{uu}^+$) plotted for various wall-normal distances ($z^+ = zU_\tau/\nu$) and as a function of timescales ($T^+ = TU_\tau^2/\nu = U_\tau^2/f\nu$). Here, U_τ and ν denote the mean friction velocity and kinematic viscosity used to normalize flow properties in viscous scaling (indicated with the superscript ‘+’). The Reynolds number of the TBL will be quantified using the friction Reynolds number, $Re_\tau = U_\tau\delta/\nu$, where δ is the TBL thickness. In figure 1, the outlined region (I) captures the energy distribution across scales associated with the Re_τ -invariant near-wall cycle [4, 5], and the associated ‘inner’ peak location is marked by a white \times for reference. Slightly larger timescales, outlined in region (II), correspond to a group of eddies/motions exhibiting distance-from-the-wall scaling (e.g. uniform momentum zones [6] or attached/wall-scaled eddies [7, 8]). The overall energy associated with region (II) is Reynolds number dependent, owing to the growth in the hierarchy/range of wall-scaled eddies with increasing Re_τ [7]. The final outlined region (III) is associated with large δ -scaled eddies or superstructures, whose energies are also dependent on the Reynolds number [5, 9, 10]. This region exhibits a peak at sufficiently high Re_τ , the approximate location for which has been marked by a white \circ for reference. A cut-off timescale of $T_C^+ = 350$ (vertical dashed line in figure 1) has often been used in the literature to nominally separate these Reynolds number dependent (u_L) and invariant (u_i) motions [11], a distinction which will be used throughout the present study to decompose u -fluctuations into $u_L = u(T^+ \gtrsim T_C^+)$ and $u_i = u(T^+ < T_C^+)$. Previous studies have generally used the terminology pairings of large- and small-scale *or* inner- and outer-scale to differentiate between these decomposed fluctuations (see [2] and [11], respectively, for example). In the present study we will use the terminology ‘large-scale’ to refer to $u_L = u(T^+ \gtrsim T_C^+)$

* mlozi2018@gmail.com

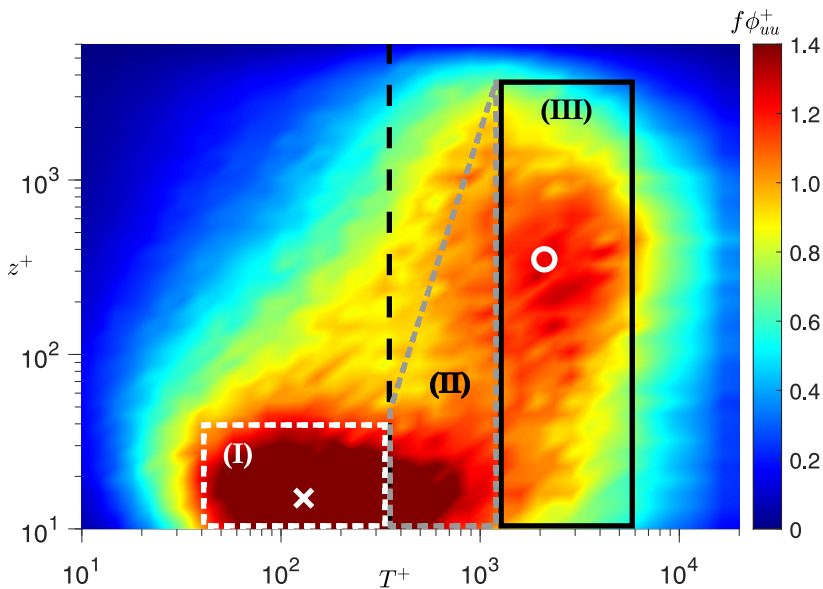


FIG. 1. Premultiplied energy spectra of a canonical TBL at $Re_\tau = 8100$ from Marusic et al. [3]. Vertical black dashed line represents the cut-off timescale $T_c^+ = 350$. The white \times and \circ mark the approximate ‘inner’ and ‘outer’ peaks respectively.

and ‘inner-scale’ to refer to $u_i = u(T^+ < T_C^+)$.

For a canonical TBL, it is now well-established that the variance of the velocity fluctuations associated with the inner scales ($\overline{u_i^{+2}}$ corresponding to region (I) of figure 1), does not vary with Re_τ [12]. Conversely, the variance of large-scale velocity fluctuations ($\overline{u_L^{+2}}$ corresponding to regions (II) and (III) of figure 1), increases with Re_τ throughout the TBL. Hence, u_L^{+2} is solely responsible for the observed Re_τ -increase in near-wall streamwise turbulence intensity in a canonical TBL [12]. Hutchins & Marusic [5] described these increasingly energetic large-scale signatures, in the near-wall region, to be a superimposition (akin to a ‘footprint’) of the structures originating in the outer region of the TBL. They also observed a large-scale modulating effect on the amplitude of small-scale (inner-scale) velocity fluctuations in the near-wall region, which was found to be reminiscent of pure amplitude modulation, and was referred to as such. Mathis et al. [2] introduced an amplitude modulation coefficient (R) to quantify this modulation of the inner scales, by the large scales, at any wall-normal location z . R was defined as:

$$R(z) = \frac{\overline{u_L^+(z)E_L(u_i^+(z))}}{\sqrt{\overline{u_L^{2+}(z)}} \sqrt{\overline{E_L(u_i^+(z))^2}}}, \quad (1)$$

where u_L^+ represents large-scale streamwise velocity fluctuations and $E_L(u_i^+)$ represents a large-scale filtered envelope of u_i computed via the Hilbert transform. Although it is agreed that two-point correlation methods give an overall higher fidelity quantification of amplitude modulation [13–15], Mathis et al. [2] demonstrated the single-point correlation coefficient in Eq. (1) yields a qualitatively similar result to the two-point correlation under most conditions. Here, it is important to take note of the fact that the amplitude modulation phenomena was originally proposed in the context of a canonical high- Re_τ TBL, to describe exclusively the effect of energetic large-scale structures superimposing onto, and modulating the amplitude of, inner scales (which are Re_τ -invariant). Per this original definition, the phenomenon is associated with an inherent sense of directionality, *i.e.* it is implied that the large-scale structure dynamics govern their non-linear interaction with the inner scales. This makes sense given that the experiments of Hutchins & Marusic [5] and Mathis et al. [2] were focused on Re_τ -effects in a canonical TBL, where the increase in amplitude modulation can be solely attributed to the Re_τ -dependent energization of the large-scale structures.

However, it is noteworthy that the existence/description of causality between large-scale superimposition and amplitude modulation is still a topic of ongoing research [16]. Previous studies have also provided alternative descriptions of the amplitude modulation phenomena for canonical TBLs, such as the quasi-steady quasi-homogeneous (QSQH) theory from Chernyshenko and co-workers [17, 18]. This theory mathematically relates the amplitude of inner-scale fluctuations in the near-wall region to large-scale fluctuations in skin friction, without making explicit assumptions about the nature of interactions between structures in the inner and outer layers (*i.e.* superimposition). As such, the ‘cause-and-effect’ relationship between amplitude modulation and large-scale motions in the near-wall region remains

an open question. The present study limits its investigation to quantifying the variation of non-linear interactions in the TBL (which include amplitude modulation) with increasing intensities of non-canonical perturbations. As a consequence, the present conclusions do not depend on the interpretation of exact physical mechanisms governing the amplitude modulation phenomena.

Based on the observations described above, the amplitude modulation phenomena can be considered as a subset of the non-linear triadic interactions coexisting across the entire TBL scale hierarchy [19]. The triadic nature of these interactions emerges from the quadratic non-linearity in the governing Navier-Stokes equations. Triadically-coupled scales correspond to the frequency scales of three eddies (say, l , m and n) that are inter-connected via any of the following relations:

$$(a) \omega_l = \omega_m - \omega_n, \quad (b) \omega_l = \omega_m + \omega_n, \quad (c) \omega_l = 2\omega_m \quad \text{or} \quad (d) \omega_l = 2\omega_n, \quad (2)$$

where, $\omega_i = 2\pi f_i = 2\pi/T_i$. Per the framework proposed by McKeon and co-workers [14, 19], the mean non-linear coupling between all triadically coupled scales (at any z) can be quantified by the skewness of the u -fluctuations, S_u . This was demonstrated by decomposing statistically stationary streamwise velocity time series, $u(t)$, into Fourier modes: $u(t) = \sum_{i=1}^{\infty} \alpha_i \sin(\omega_i t + \psi_i)$, with amplitudes (α_i), phase (ψ_i) and $0 < \omega_i < \omega_{\infty}$. Hence,

$$S_u = \frac{\overline{u^3}}{\sigma^3} = \frac{6}{4\sigma^3} \sum_{\substack{\forall l, m, n \\ \omega_l < \omega_m < \omega_n \\ \omega_l + \omega_m = \omega_n}} \alpha_l \alpha_m \alpha_n \sin(\psi_l + \psi_m - \psi_n) + \frac{3}{4\sigma^3} \sum_{\substack{l=1 \\ \omega_n = 2\omega_l}} \alpha_l^2 \alpha_n \sin(2\psi_l - \psi_n), \quad (3)$$

where $\sigma = \sqrt{\overline{u^2}}$, and $\psi_l + \psi_m - \psi_n$ represents the phase difference between triadically coupled scales. Based on Eq. (3), S_u can be considered a surrogate for the average measure of phase difference between triadically coupled scales across the full spectrum of energetic turbulent eddies/motions [19]. Thus, higher S_u can be interpreted as a stronger coupling/interaction owing to a lower phase lag between triadically coupled scales. Consideration of skewness to quantify inter-scale coupling is also useful because it does not require any normalization, which can otherwise undermine comparisons between datasets covering a broad range of non-canonical characteristics.

The inter-scale interactions can be understood in more detail by computing the individual (small) inner- ($u_i = u(T^+ < T_c^+)$) and (outer) large- ($u_L = u(T^+ > T_c^+)$) scale contributions to S_u , where the cut-off timescale considered is $T_c^+ = 2\pi/\omega_c^+ = 350$ [11]. This decomposition based on frequency cut-off (instead of a wavelength-based cut-off) is preferred, given it avoids dependence on the choice of convective velocity, which may influence the amplitude modulation coefficient [20]. This decomposition enables estimation of the non-linear coupling between u_L and u_i , for which we substitute $u = u_L + u_i$ into (3) following Mathis et al. [21] to obtain:

$$S_u = \frac{\overline{u^3}}{\sigma^3} = \overline{u^3} = \overline{u_L^3} + \overline{u_i^3} + 3\overline{u_L^2 u_i} + 3\overline{u_i^2 u_L}, \quad (4)$$

where the double overbar denotes a time-averaged quantity normalised by σ^3 . Duvvuri and McKeon [19] reported exact expressions for the individual terms in Eq. (4), with

$$\overline{u_i^2 u_L} = \frac{1}{2\sigma^3} \sum_{\substack{\forall l, m, n \\ \omega_n - \omega_m = \omega_l \\ 0 < \omega_l < \omega_c \\ \omega_m, \omega_n > \omega_c}} \alpha_l \alpha_m \alpha_n \sin(\psi_l + \psi_m - \psi_n) = \frac{R}{2} \left(\sqrt{\overline{u_L^{2+}(z)}}} \sqrt{\overline{E_L(u_i^+(z))^2}} \right), \quad (5)$$

indicating that the ‘cross-term’ $3\overline{u_i^2 u_L}$ represents the mean phase difference between the large scales ω_l and an ‘envelope’ of the triadically-coupled inner scales: $\omega_n, \omega_m (> \omega_c)$. Increasing values for this cross-term are therefore associated with a stronger inter-scale coupling/interaction owing to a reduction in phase between u_L and u_i . Mathis et al. [21] observed experimentally that $3\overline{u_i^2 u_L}$ behaved similarly to the correlation coefficient (R) used to quantify the amplitude modulation phenomena, and was also the most dominant scale-decomposed skewness term (Eq. 4) for a canonical TBL. Additionally, this cross-term had a strong Reynolds number dependence that extended across the whole TBL, akin to the behaviour of R . The direct proportionality between the cross-term and the amplitude modulation coefficient (R) was formally established by Duvvuri & McKeon [19] through Eq. (5), thereby also confirming R to represent a subset of the non-linear interactions coexisting across the full TBL scale hierarchy.

A number of studies have also used the correlation coefficient from Eq. (1) to quantify the inter-scale coupling in non-canonical TBLs. The results from these non-canonical studies are often interpreted such that any increment in R is an artefact of amplitude modulation, in the classical sense defined by Mathis et al. [2] (*i.e.* driven by changes in the large-scale dynamics). However, inter-scale coupling measured in most, if not all, non-canonical TBLs can pertain

TABLE I. Published hot-wire datasets considered in the present study

Hot-Wire Dataset	Baseline Canonical TBL	Perturbation	Magnitude	Hot-wire resolution
Marusic et al. [3]	Smooth-Wall ZPG, $Re_\tau \approx 2800$	Increasing Re_τ	$2800 < Re_\tau < 13400$	$l^+ \sim 24$
Deshpande et al. [25]	Smooth-Wall ZPG, $Re_\tau \approx 6500$	Increasing APG	$0.0 < \beta < 1.7$	$l^+ \sim 10$
Squire et al. [29]	Smooth-Wall ZPG, $Re_\tau \approx 6500$	Increasing surface roughness	$0 < k_s^+ < 97$	$l^+ \sim 22$
Deshpande et al. [11]	Smooth-Wall ZPG, $Re_\tau \approx 6000$	Increasing spanwise wall forcing	$0.0 \leq A^+ \leq 12.3$, $0.000 \leq f_{osc}^+ \leq 0.007$	$l^+ \sim 8$
Abbassi et al. [30]	Smooth-Wall ZPG, $Re_\tau \approx 14400$	u_L Opposing jet	–	$l^+ \sim 20$
Abbassi et al. [30]	Smooth-Wall ZPG, $Re_\tau \approx 14400$	u_L Reinforcing jet	–	$l^+ \sim 20$

to interactions beyond the specific subset of interactions which correspond to amplitude modulation (defined in Eqs. 1–5). For instance, the classical definition of amplitude modulation would preclude describing changes in inter-scale coupling in flows without an energetic large-scale structure, as amplitude modulation (*i.e.* ZPG TBLs at $Re_\tau \lesssim \mathcal{O}(10^2)$ [5], where regions (II) and (III) of figure 1 are statistically insignificant). Similarly, it would also be incorrect to describe changes in inter-scale coupling as amplitude modulation if they are solely associated with manipulation of the near-wall cycle (*i.e.* region (I) in figure 1), that occurs owing to non-canonical effects such as roughness [22] or porous surfaces [23]. Interestingly, other non-canonical effects such as pressure gradients [24, 25], thermal stratification [26] or large-scale free-stream disturbances [27] have also been found to be responsible for affecting the entire hierarchy of turbulent scales (*i.e.* across regions (I)-(III) in figure 1). However, associating the corresponding changes in inter-scale coupling solely with the amplitude modulation phenomena would not be appropriate, given they are likely to be an artefact of changes in both u_L and u_i , differing from the classical definition. Additionally, in all the above non-canonical scenarios, the inherent uni-directionality associated with the amplitude modulation phenomena (regarding large-scale structure dynamics affecting the inner scales) may not be strictly applicable.

II. EXPERIMENTAL DATASETS

In the present study, we argue that changes in the modulation coefficient, R , or the cross-term, $\overline{3u_i^2 u_L}$, alone are insufficient to draw conclusions regarding changes in the amplitude modulation phenomena. For this, we have assembled and analyzed a unique set of published hot-wire datasets from the large Melbourne wind tunnel facility. These datasets will be used to demonstrate enhancement of the inter-scale TBL couplings owing to various non-canonical perturbations, and used for rigorous evaluation with respect to the classical definition of amplitude modulation given by Mathis et al. [2]. The measurement details of all these datasets can be found in their respective references, which have been documented alongside the range of their respective perturbations in table I. Each of these datasets comprise a canonical baseline case, *i.e.* corresponding to a high- Re_τ ZPG TBL over a smooth wall, against which the effect of each perturbation, on inter-scale coupling, will be analyzed at matched TBL Re_τ . A unique aspect of these datasets is that each of them is acquired with nominally similar hot-wire resolution l^+ , ensuring that the effect of spatial filtering emerging from finite hot-wire length (l ; [12]) will not adversely affect our conclusions. To that end, the datasets in table I have been re-analyzed using the framework described in Eqs. (1)–(5) and the compiled results are presented in figures 2 and 3. The normalized inner- and large-scale contributions to the variance of streamwise velocity fluctuations ($\overline{u_i^{2+}}$ and $\overline{u_L^{2+}}$, respectively), estimated based on $T_C^+ = 350$, will be used to identify the scale range and wall-normal regions that are affected by each perturbation. These conclusions, however, should not be influenced by the choice of a viscous-scaled frequency cut-off (T_C^+ ; [2]) since every non-canonical case is compared against its canonical baseline case at matched Re_τ (refer to table I). Complimenting the variance, the premultiplied energy spectra from the near-wall and outer regions will also be presented to corroborate our discussion based on $\overline{u_i^{2+}}$ and $\overline{u_L^{2+}}$. All these statistics as well as their reference z -locations have been normalized using the friction velocities (U_τ) associated with the respective perturbed cases. The choice of U_τ , however, does not affect the main conclusions that will be based predominantly on the skewness terms Eq. (4). These terms are considered to analyze the effect of non-canonical perturbations on the various triadic interactions coexisting in the near-wall region of the TBL. Particular attention is given to the near-wall region since several past efforts have focused on leveraging inter-scale interactions to predict the turbulence characteristics in this region [28], which is often inaccessible in high- Re_τ experiments. In figures 2 and 3, variances and non-linear coupling terms associated with the canonical baseline cases have been plotted using light shading and a solid black outline, for all cases considered in table I.

III. NON-LINEAR INTERACTIONS FOR VARYING PERTURBATION INTENSITIES

A. Increasing Reynolds number, Re_τ

The first dataset is from the canonical TBL study of Marusic et al. [3], where the perturbation of interest is an increase in the flow Re_τ . In this experiment, increasing Re_τ values were achieved by maintaining a nominally constant upstream flow condition and conducting hot-wire measurements at various downstream locations, to achieve an increase in Re_τ without significant changes to the viscous scale. It is noteworthy that this specific perturbation formed the original description of amplitude modulation by Mathis et al. [2], where the Re_τ -increase in the energy of large-scale velocity fluctuations in regions (II) and (III) (of figure 1) led to an increase in the coupling (reduction in phase difference) between the inner- and large-scaled velocity fluctuations [2, 11].

Statistics from the Marusic et al. [3] dataset are presented in figures 2.1. As expected based on the literature [12], there is no change in $\overline{u_i^{+2}}$ with increasing Re_τ (light to dark colors in figure 2.1a), while a significant change in $\overline{u_L^{+2}}$ can be seen across all z^+ -locations. The premultiplied spectra in figure 2.1b are from $z^+ = 15$, as indicated by the vertical dotted line in figure 2.1a. The only significant change in the spectra is an increase in energy corresponding to the large scales (right of vertical dotted line at $T_C^+ = 350$), *i.e.* corresponding to an increase in u_L -energy. A similar effect is seen in the premultiplied spectra in figure 2.1d which are from $z^+ = 200$ (*i.e.* in the log region), indicated by the vertical dash-dotted line in figure 2.1a. The effect of increasing Re_τ on the skewness and the cross-term can be seen in figures 2.1c,e. Consistent positive changes in the skewness and cross-term, with increasing Re_τ , are observed for both z -locations. The assertion that amplitude modulation (*i.e.* the cross-term) is the only statistically significant triadic/non-linear interaction for a canonical TBL is confirmed by the similar magnitudes of the skewness and the cross-term in figures 2.1c,e. This is reaffirmed in figures 3.1a,b which demonstrate a negligible variation in all other terms of Eq. (4) with increasing Re_τ (also shown by [21]), thereby suggesting insignificant changes in other triadic interactions with increasing Re_τ .

B. Increasing APG strength, β

The second dataset is from Deshpande et al. [25] where the perturbation is a low-to-moderate adverse-pressure gradient (APG) with increasing strength as quantified by the Clauser pressure-gradient parameter, β . Here, $\beta(x) = (\delta^*/\rho U_\tau^2) (dP/dx)$, where $\delta^* = \int_0^\delta (1 - U(z)/U_e) dz$ is the displacement thickness, $U(z)$ is the mean streamwise velocity at wall-normal location z , $U_e = U(z = \delta)$, *i.e.* the edge velocity, ρ is the fluid density and dP/dx is the mean streamwise pressure-gradient at the measurement location x . In this experiment, increasing β values were achieved by systematically increasing the number of low-porosity screens installed at the tunnel outlet. The presence of these screens increased the tunnel static/back pressure, while openings along the test section roof permitted the pressurized air to bleed out from various streamwise locations, thereby imposing a moderately strong APG on the TBL developing along the bottom wall [25]. A single hot-wire measurement station (located near the downstream end of the test section to ensure a nominal high- Re_τ condition) was used, and the free-stream velocity at this location was matched for various β -cases to ensure a nominally matched Re_τ . Based on the conclusions of Deshpande et al. [25], such a perturbation is expected to increase the energy of both the inner- and large-scale velocity fluctuations, especially in the outer-region of the TBL.

Velocity statistics associated with the various APG cases are presented in figures 2.2. In figure 2.2a, a distinct increase in $\overline{u_i^{+2}}$ can be seen in the outer region for all APG cases (relative to the ZPG case), while it does not change significantly in the inner region. This is well-known in the literature [25, 31] for weak and moderately strong APG TBLs, with the behaviour in the outer region being associated with the migration of the near-wall ‘inner’ scales to the outer region [32]. Changes in $\overline{u_L^{+2}}$ can also be seen across all z^+ -locations, specifically an increase in the outer region ($z^+ > 200$) can be noted that is proportional to β [25, 31]. The premultiplied spectra in figure 2.2b are from $z^+ = 24$, as indicated by the vertical dotted line in figure 2.2a. This is the z^+ -location nearest to the wall where data was available for each case, including the baseline canonical case. The only discernible change is an increase in the premultiplied spectra amplitude for large scales (right of vertical dotted line at $T_C^+ = 350$), which is associated with an increase in β . The premultiplied spectra in figure 2.2d are from $z^+ = 1000$, where the largest pressure gradient related changes to the variance are observed, indicated by the vertical dash-dotted line in figure 2.2a. At this z^+ -location there is a broadband increase in the premultiplied spectra amplitude, corresponding with an increase in β , however the amplitude of inner scales ($T^+ < T_C^+$) does not change significantly with increasing β for $\beta \gtrsim 0.9$, similar to the trend seen in $\overline{u_i^{+2}}$ in figure 2.2a.

The effect of increasing β on the skewness and the cross-term has been documented in figures 2.2c,e. Both these terms exhibit net growth with increasing β , at the inner as well as outer z^+ -locations. This effect can be seen for

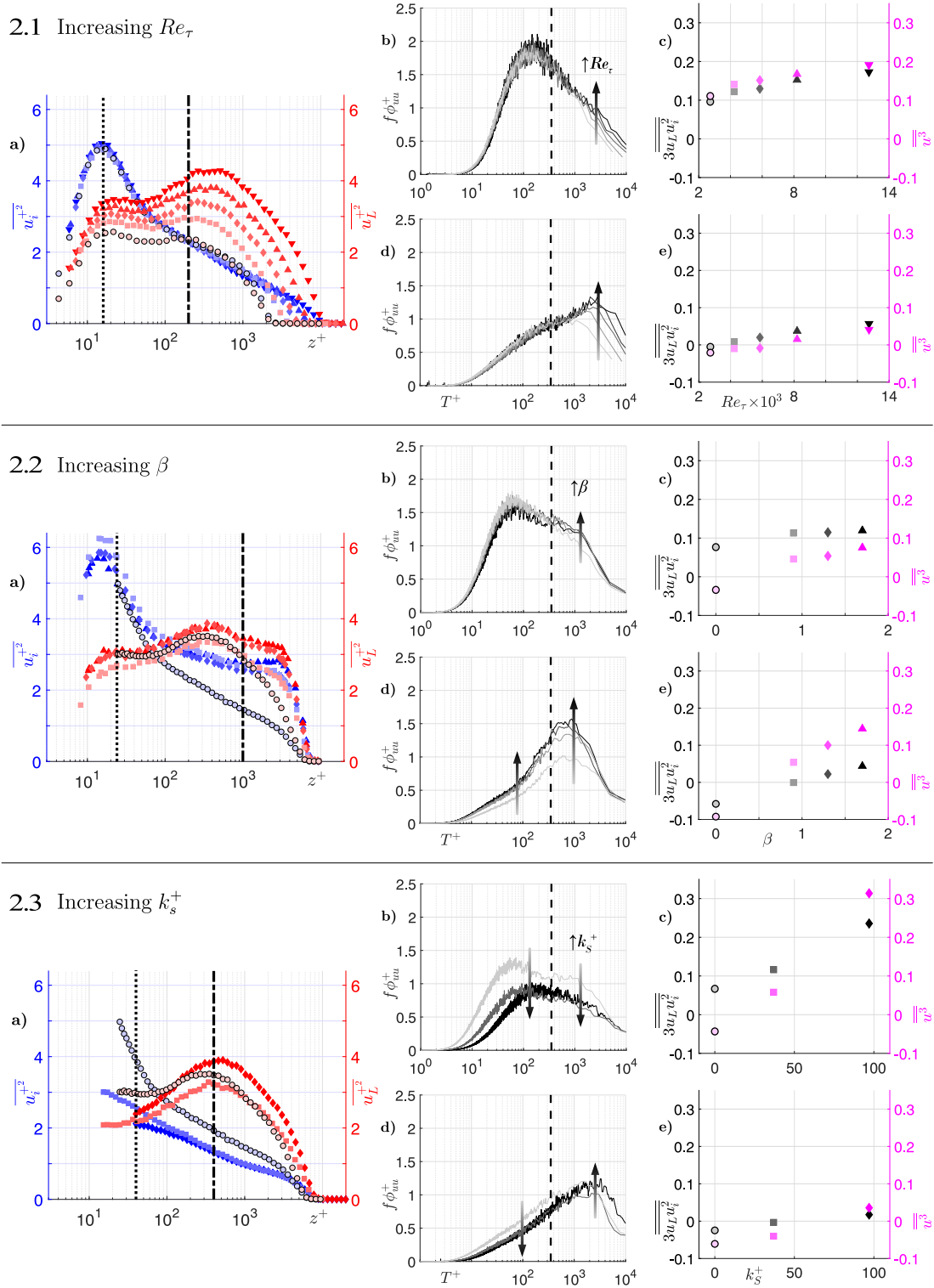
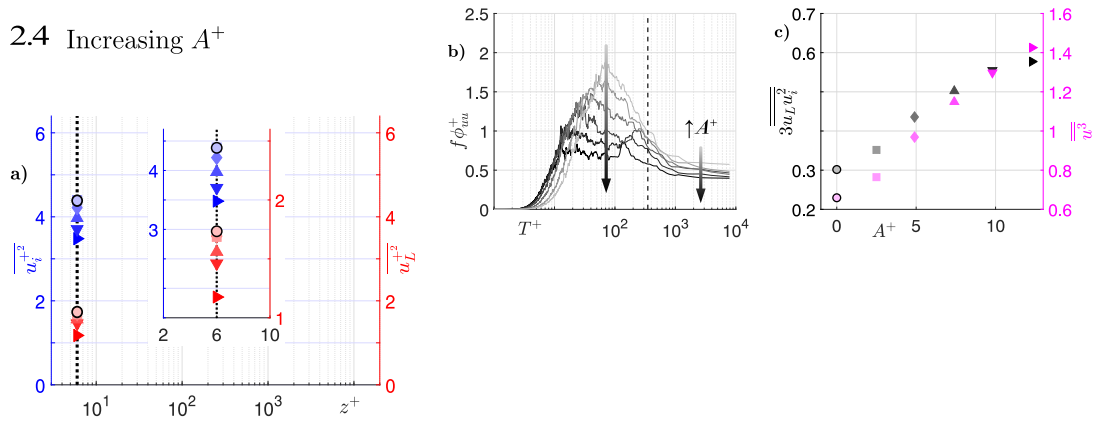
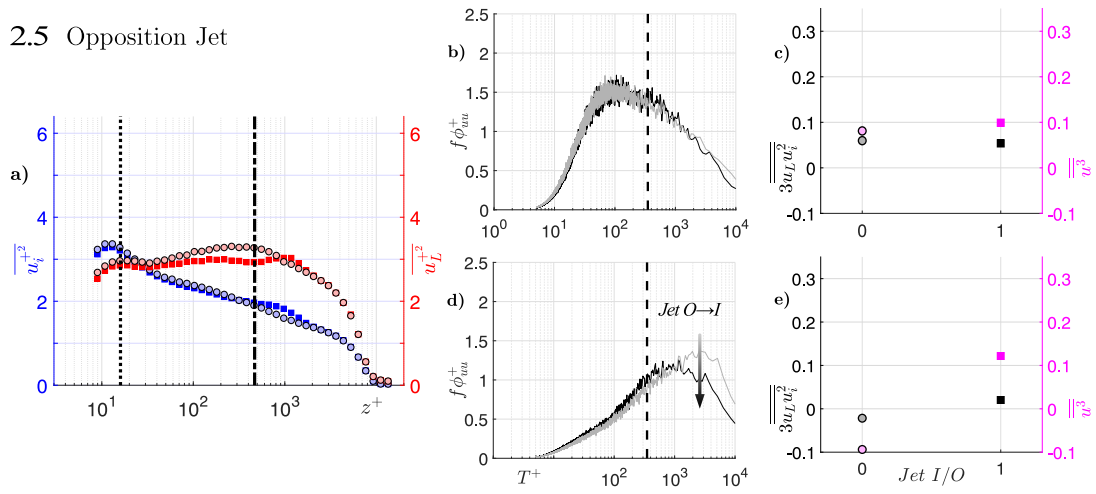


FIG. 2. (left column) Variance of inner- (left axis) and large- (right axis) scale velocity fluctuations for varying intensities of the following perturbations: **2.1** Increasing Re_τ , **2.2** Increasing β and **2.3** Increasing k_s^+ . (center column) Premultiplied energy spectra for z^+ -locations corresponding to (b) the inner region (indicated by a vertical dotted line in (a)) and (d) the outer region (indicated by a dash-dotted line in (a)). Vertical dashed lines in the center column represent the cut-off timescale, $T_c^+ = 350$. (right column) Cross-term, $3\overline{u_L u_i^2}$, (left axis) and skewness of streamwise velocity fluctuations, $\overline{u^3}$ (right axis) as a function of increasing perturbation intensities at z^+ -locations, matched with (b,d) respectively, corresponding to (c) the inner region and (e) the outer region. Reference canonical cases are shown in the lightest shading, and symbols for the reference canonical cases have a solid black outline.

2.4 Increasing A^+ 

2.5 Opposition Jet



2.6 Reinforcing Jet

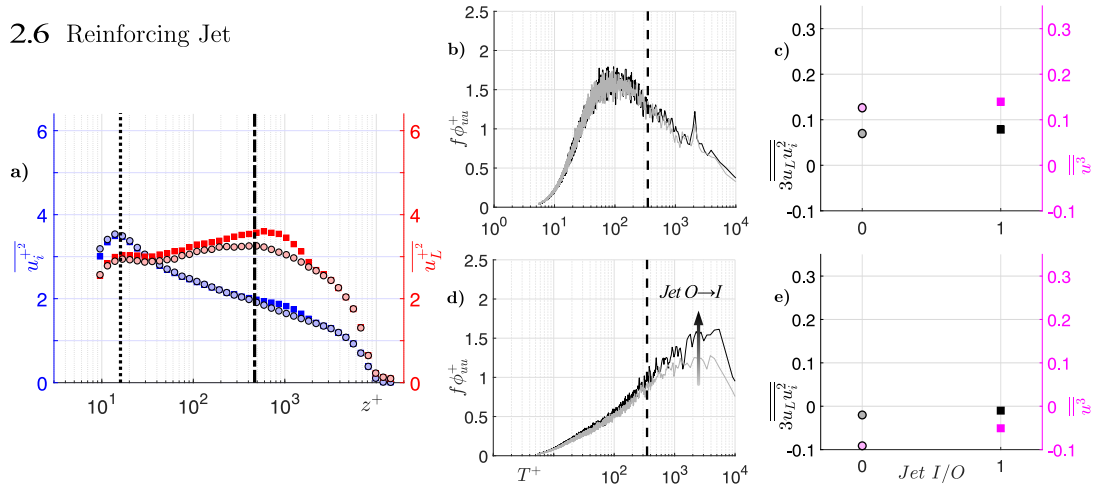


FIG. 2. (*continued*) – (*left column*) Variance of inner- (left axis) and large- (right axis) scale velocity fluctuations for varying intensities of the following perturbations: **2.4** Increasing A^+ , **2.5** Opposition jet and **2.6** Reinforcing jet. (*center column*) Premultiplied energy spectra for z^+ -locations corresponding to (b) the inner region (indicated by a vertical dotted line in (a)) and (d) the outer region (indicated by a dash-dotted line in (a)). Vertical dashed lines in the center column represent the cut-off timescale, $T_c^+ = 350$. (*right column*) Cross-term, $\overline{3u_L u_i^2}$, (left axis) and skewness of streamwise velocity fluctuations, $\overline{u^3}$ (right axis) as a function of increasing perturbation intensities at z^+ -locations, matched with (b,d) respectively, corresponding to (c) the inner region and (e) the outer region. Reference canonical cases are shown in the lightest shading, and symbols for the reference canonical cases have a solid black outline.

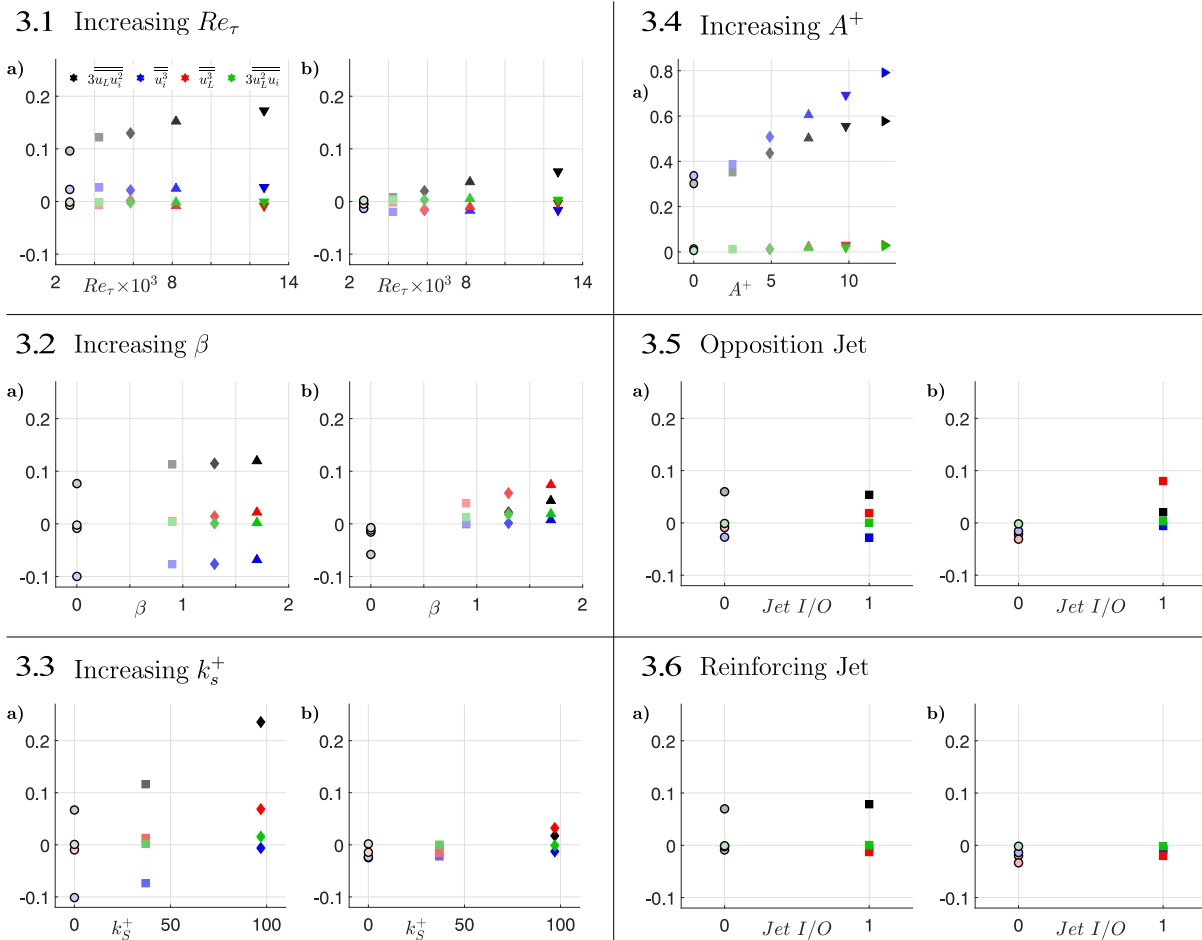


FIG. 3. Cross-terms ($3\overline{u_L u_i^2}$, $3\overline{u_L^2 u_i}$) and skewness of inner- and large-scale velocity fluctuations ($\overline{u_i^3}$, $\overline{u_L^3}$) as a function of increasing perturbation intensities at z^+ -locations corresponding to (a) the inner region (vertical dotted lines) and (b) the outer region (dash-dotted lines) as indicated in the corresponding subfigures (a) in figure 2. Results from reference canonical cases are shown in the lightest shading, and have a solid black outline.

all APG strengths in the dataset, ranging from a relatively weak APG ($\beta < 1$, square symbols) to a moderate APG ($\beta \sim 1.7$, triangle symbols). However, unlike the case of canonical TBLs, there are noticeable differences between the magnitudes of the skewness and the cross-term, and their rate of increase with β , suggesting changes in triadic interactions apart from those associated with the amplitude modulation phenomena. This is evidenced in figures 3.2a,b where both $\overline{u_L^3}$ and $\overline{u_i^3}$ are noted to increase with β , particularly rapidly in the outer region. This enhancement can be associated with the energization of the inner and large scales by the APG, as discussed above [31, 32]. It confirms the influence of APG on the non-linear interactions spanning across the entire scale hierarchy coexisting in the TBL. These results suggest that, within the framework of increasing APG strength (β) as a perturbation to the baseline canonical TBL, enhancement of all the triadic coupling needs to be accounted for in any predictive models for APG TBLs. Moreover, the uni-directionality associated with the amplitude modulation phenomena (*i.e.* u_L governing inter-scale interactions) cannot be extended to APG TBLs given both u_L and u_i are manipulated with increasing β (figure 2.2a).

C. Increasing surface roughness, k_s^+

The third dataset is from Squire et al. [29], where the perturbation is increasing surface roughness characterized by an increasing Nikuradse-roughness height, k_s^+ . In this experiment, the entire tunnel floor was covered with a P36 grit sandpaper, while both the free-stream velocities and streamwise measurement locations were adjusted such that a nominally constant high- Re_τ was maintained across various k_s^+ cases. This also meant that k_s/δ increased with k_s^+ , however, the relative roughness height consistently remained small across all cases (*i.e.* $\delta/k_s \gtrsim 40$).

Based on the conclusions of Squire et al. [29], surface roughness is expected to decrease the energy of both the inner- and large-scale velocity fluctuations near the wall. As such, this perturbation directly affects the TBL region (I) labelled in figure 1, and this is confirmed from the hot-wire statistics presented in figures 2.3. In figure 2.3a, there is a significant decrease in $\overline{u_i^{+2}}$ with increasing k_s^+ (light to dark colors) across all z^+ -locations. There is also a decrease in $\overline{u_L^{+2}}$, which is primarily localized to the near-wall region ($z^+ < 100$). The premultiplied spectra in figure 2.3b are plotted for $z^+ \approx 40$, which was the nearest possible location for hot-wire data acquisition amongst all roughness cases considered. The amplitude of the premultiplied spectra is noted to decrease across all scales (*i.e.* all T^+) with an increase in k_s^+ . This confirms that there is a decrease in the energy of both u_i and u_L near the wall, corresponding with the increase in k_s^+ . The premultiplied spectra in figure 2.3d are plotted for $z^+ = 400$ (*i.e.* in the log region). At this location there is still a decrease in the energy of inner scales (left of vertical dotted line at $T_C^+ = 350$), but there is now an increase in the energy of large scales (right of vertical dotted line at $T_C^+ = 350$), associated with the largest k_s^+ . These spectra highlight the unique aspects of the surface roughness perturbation which set it apart from the previous two cases.

The effect of increasing k_s^+ on the skewness and the cross-terms are shown in figures 2.3c.e. Both the skewness and the cross-term show a positive change with increasing k_s^+ , which can be seen across both transitionally rough ($0 < k_s^+ < 80$; square symbols) and fully-rough scenarios ($k_s^+ > 80$; diamond symbols), at both z^+ -locations. These results suggest that, within the framework of increasing surface roughness (k_s^+) as a perturbation to the baseline canonical TBL, a decrease in energy of both inner and large scales is associated with a local increase in the magnitude of inter-scale coupling near the wall. Similarly, a decrease in energy of inner scales and an increase in the energy of large scales is also associated with a local increase in the magnitude of inter-scale coupling in the log region. Although this increase in the cross-term near the wall resembles an amplitude modulation effect, it differs fundamentally from the original definition by Mathis *et al.* [2] for a canonical TBL. In the case of increasing k_s^+ , notably, magnitudes of both u_i and u_L are reduced in the near-wall region, and thus the increase in the cross-term cannot solely be attributed to the influence of the large scales. Further, increasing k_s^+ is found to influence the non-linear interactions spanning the entire energy spectrum, especially near the wall, which is evident from the various decomposed terms of skewness plotted in figure 3.3a,b. Therefore, akin to the effect of increasing β , the current analysis indicates the need to account for all non-linear triadic interactions in the development of future data-driven predictive models for a rough wall TBL. Moreover, the growth of the cross-term cannot be characterized as an amplitude modulation effect in the traditional sense as defined by Mathis et al. [2].

Although the present analysis limits itself to scenarios of TBL developing over homogeneously distributed surface roughness, further interesting flow characteristics can be expected if step changes in surface roughness are considered. Interested readers are referred to the recent study by Li et al. [33], who have experimentally quantified the cross-term (*i.e.*, amplitude modulation term) for a TBL developing after a rough-to-smooth change in wall condition. Their investigation revealed higher magnitudes of the cross-term in the near-wall region (relative to a canonical TBL), which was attributed to the more energetic footprints of the large-scale motions influenced by the upstream rough-wall condition.

D. Increasing spanwise wall forcing, A^+

The fourth dataset considered here is from Deshpande et al. [11] where the perturbation is a spanwise oscillating wall with increasing magnitude of the spanwise wall velocity, given by $A^+ = A/U_\tau$. In this experiment, forty-eight individual slats mounted along a 2.4 m portion of the test section floor were oscillated in a phase-synchronized manner along the spanwise direction, leading to the creation of an 8λ long upstream-traveling sinusoidal wave with user specified frequencies (f_{osc}). With a nominal stroke length ($d = 18\text{ mm}$) for the slat movement, the amplitude of the spanwise wall velocity ($A = 2\pi d f_{osc}$) could be varied by changing the user specified oscillation frequency. For the experiments considered in this study, the wall oscillation frequency range was maintained between $0.000 \leq f_{osc}^+ \leq 0.007$, which led to a variation in spanwise wall forcing across $0.0 \leq A^+ \leq 12.3$. Hot-wire measurements were conducted in the very near-wall region, above the oscillating slats, for both the non-actuated and actuated cases. The wind tunnel free-stream velocity was matched in all cases.

Based on the findings of Deshpande et al. [11], this wall actuation attenuates the energy of both inner- and large-scale velocity fluctuations, thereby affecting the energy spectra across regions (I)–(III) of figure 1. The hot-wire statistics from these cases are presented in figures 2.4, which although limited to a single z^+ -location, exhibit trends consistent with other locations in the near-wall region (confirmed by comparisons with independent PIV measurements in [34]). As seen in figure 2.4a, a significant decrease in both $\overline{u_i^{+2}}$ and $\overline{u_L^{+2}}$ with increasing A^+ (light to dark colors) at $z^+ = 6$ is observed. This is confirmed by figure 2.4b, which shows an attenuation of the amplitude of the premultiplied spectra across all $T^+ \gtrsim 50$, with increasing A^+ . The effect of increasing A^+ on the skewness and the cross-term at $z^+ = 6$ is shown in figure 2.4c, where both these statistics are found to exhibit a significant positive change with increasing A^+ (*i.e.*, increasing drag reduction [11, 34]). Similar observations of increasing skewness, with

increasing drag reduction, have been noted previously on introduction of local oscillating blowing [35] or microbubbles and polymers [36] in the TBL. However, none of these studies associated their observations with inter-scale interactions, which has been discussed here. A notable observation in the present study is the gradual positive change in the non-linear interactions, starting from the smallest perturbation/ A^+ (in square symbols), through to the largest perturbation/ A^+ (right pointing triangle symbols). These results suggest that, within the framework of increasing spanwise wall forcing as a perturbation to the baseline canonical TBL, the decrease in near-wall energy of both inner and large scales is accompanied with a significant local increase in the inter-scale coupling. However, similar to the case of surface roughness, the present increase in the cross-term cannot be associated with the amplitude modulation defined in the classical sense, given it is a consequence of attenuation of both large and inner scales. Further, significant differences between the magnitudes, and rate of increase, of the cross-term and skewness in figure 2.4c can be explained by the increasing magnitude of only the $\overline{u_i^3}$ term (with increasing A^+) as shown in figure 3.4a, but not of $\overline{u_L^3}$. Collectively, all the aforementioned cases reveal the uniqueness with which different perturbations manipulate the various triadic interactions coexisting in the TBL.

E. Opposing and reinforcing wall-normal jet forcing

The fifth and sixth datasets are from Abbassi et al. [30], where the perturbation is a wall-normal jet with a control scheme designed to either enhance (reinforcing case) or weaken (opposition case) large-scale velocity fluctuations in the outer region. In these experiments, a spanwise array of hot-film sensors placed on the wall, upstream of the jet-actuators, were used to identify the footprint of incoming u_L motions as an input for the actuation scheme. The actuators were composed of a spanwise array of streamwise elongated slots in the wall, which generated a wall-normal jet of pressurized air supply that penetrated into the log region of the TBL. A single hot-wire measurement station downstream of the jets was used, and the free-stream velocity was matched in both the actuated and non-actuated cases to maintain a nominally similar high- Re_τ inflow condition. In the opposition control case, the hot-film sensors were used to identify incoming high-energy ($+u_L$) large-scale motions so the jets could fire against these high-skin-friction-contributing regions [30]. On the other hand, the same system was used to identify and target incoming low-energy ($-u_L$) large-scale motions for the reinforcing case.

Abbassi et al. [30] found the opposing and reinforcing cases to respectively attenuate and enhance the large-scale energy in the outer region. This is indeed depicted by $\overline{u_L^{+2}}$ presented in figures 2.5a and 2.6a for the opposition and reinforcing cases respectively, while $\overline{u_i^{+2}}$ remains relatively unaffected for both. Hence, both these cases represent a unique scenario where a change in the large-scale energy in the outer region is not reflected in their signatures/footprints close to the wall. This is supported by the premultiplied spectra plotted for both the reinforcing (figure 2.5b) and opposing cases (figure 2.6b) compared against their corresponding non-actuated cases at $z^+ \approx 15$. Consequently, the effects of either of these wall-normal jet forcings, on the skewness and the cross-terms, are negligible at $z^+ = 15$ (depicted in figures 2.5c and 2.6c). Alternatively, the premultiplied spectra plotted for the reinforcing (figure 2.5d) and opposing cases (figure 2.6d) at $z^+ \approx 500$ (*i.e.* in the log region) show a decrease or increase in the energy of large scales (right of vertical dotted line at $T_C^+ = 350$) corresponding with the forcing scheme and reflected in $\overline{u_L^{+2}}$ in figures 2.5a,6a. Now at $z^+ \approx 500$ the effects of these wall-normal jet forcings, especially the opposition jet, on the skewness and the cross-terms, are discernible in figures 2.5e,6e). Further, figures 3.5 and 3.6 demonstrate that the $\overline{u_L^3}$ term of Eq. (4) is most strongly influenced by the jet forcings, while there is a negligible influence on any other non-linear couplings, especially in the near-wall region (in a statistically-averaged sense). Hence, both the present jet forcing cases suggest the possibility of a unique scenario where near-wall non-linear couplings remain unaffected despite the large-scale fluctuations in the outer region being energized/attenuated. It suggests that not every large-scale phenomena in the outer region influences the near-wall region, and hence the prediction of the near-wall signatures for such complex non-canonical effects may not be as straightforward as for canonical TBLs.

IV. SUMMARY AND CONCLUSIONS

This study evaluates the connection between inter-scale interactions in non-canonical TBLs with the amplitude modulation phenomenon observed by Mathis et al. [2] for canonical wall-bounded flows. Published hot-wire datasets corresponding to various non-canonical effects are considered, including surface roughness, adverse-pressure gradients, spanwise and wall-normal forcing, each of which are associated with unique changes in the inner- and large-scale energy (relative to their canonical baseline cases). These changes, as documented in table II, are responsible for distinguishing their inter-scale interactions from the classical definition of amplitude modulation conceived by Mathis et al. [2], for scenarios of increasing Re_τ (wherein the interaction is solely governed by changes in u_L). The present study unravels a clear distinction between the range of triadically-coupled scales and wall-normal TBL regions that are influenced

TABLE II. Summary of key findings based on figures 2 and 3. \uparrow and \downarrow respectively indicate increase or decrease in magnitude relative to their canonical base cases.

Perturbation	TBL region	$\overline{u_i^2}$	$\overline{u_L^2}$	$\overline{\overline{u_i^2 u_L}}$	$\overline{\overline{u_i^3}}$	$\overline{\overline{u_L^3}}$	$\overline{\overline{u_L^2 u_i}}$
Increasing Re_τ	inner	\approx	\uparrow	\uparrow	\approx	\approx	\approx
	outer	\approx	\uparrow	\uparrow	\approx	\approx	\approx
Increasing β	inner	\approx	\uparrow	\uparrow	\uparrow	\uparrow	\approx
	outer	\uparrow	\uparrow	\uparrow	\uparrow	\uparrow	\approx
Increasing k_s^+	inner	\downarrow	\downarrow	\uparrow	\uparrow	\uparrow	\approx
	outer	\downarrow	\uparrow	\uparrow	\approx	\uparrow	\approx
Increasing A^+	inner	\downarrow	\downarrow	\uparrow	\uparrow	\approx	\approx
Opposing u_L	inner	\approx	\approx	\approx	\approx	\approx	\approx
	outer	\approx	\downarrow	\uparrow	\approx	\uparrow	\approx
Reinforcing u_L	inner	\approx	\approx	\approx	\approx	\approx	\approx
	outer	\approx	\uparrow	\uparrow	\approx	\uparrow	\approx

by the increasing intensities of different non-canonical perturbations (table II). This underscores the necessity of quantifying these interactions across a broad scale hierarchy, via dedicated two-point correlations, when constructing predictive models for non-canonical flows.

Interestingly, it was observed that several (though not all) perturbation effects led to an enhancement of inter-scale coupling and broadband changes in the velocity spectra, with increasing perturbation intensities (table II). This observation is consistent with past studies [11, 34, 37] and highlights the tendency of turbulence scales to align more closely (*i.e.*, exhibit reduced phase lag) when subjected to certain external forcings/perturbations. In terms of flow physics, the manipulation of inter-scale coupling in non-canonical flows could be feasibly linked with changes in scale-dependent inclination angles of coherent structures [38, 39]. Previous research in canonical flows [14, 39] has already indicated these angles to be governing inter-scale phase relationships. Alternatively, unique perspectives such as the QSQH theory [17, 18] may also be able to explain some of the changes in inter-scale interactions noted here for non-canonical TBLs. This collectively encourages a more thorough exploration of wall turbulence from a dynamical systems perspective [19, 37].

We gratefully acknowledge A/Prof. Ian Jacobi for insightful discussions, and the assistance of Dr. Reza Abbassi and Dr. Dougal Squire with regards to accessing the published experimental datasets. R. D. is grateful for financial support from the University of Melbourne’s Postdoctoral Fellowship. R. D. and I. M. gratefully acknowledge funding from the Office of Naval Research (ONR) and ONR global grant: N62909-23-1-2068.

AUTHOR CONTRIBUTIONS

Mitchell Lozier: Writing – original draft, Investigation, Methodology, Validation, Formal analysis.

Ivan Marusic: Conceptualization, Writing – review & editing, Funding acquisition, Supervision.

Rahul Deshpande: Conceptualization, Methodology, Writing – review & editing, Funding acquisition, Supervision.

-
- [1] P. R. Bandyopadhyay and A. Hussain, The coupling between scales in shear flows, *The Physics of Fluids* **27**, 2221 (1984).
 - [2] R. Mathis, N. Hutchins, and I. Marusic, Large-scale amplitude modulation of the small-scale structures in turbulent boundary layers, *Journal of Fluid Mechanics* **628**, 311 (2009).
 - [3] I. Marusic, K. A. Chauhan, V. Kulandaivelu, and N. Hutchins, Evolution of zero-pressure-gradient boundary layers from different tripping conditions, *Journal of Fluid Mechanics* **783**, 379 (2015).
 - [4] S. J. Kline, W. C. Reynolds, F. A. Schraub, and P. W. Runstadler, The structure of turbulent boundary layers, *Journal of Fluid Mechanics* **30**, 741 (1967).
 - [5] N. Hutchins and I. Marusic, Evidence of very long meandering features in the logarithmic region of turbulent boundary layers, *Journal of Fluid Mechanics* **579**, 1 (2007).
 - [6] R. J. Adrian, C. D. Meinhart, and C. D. Tomkins, Vortex organization in the outer region of the turbulent boundary layer, *Journal of Fluid Mechanics* **422**, 1 (2000).

- [7] J. Hwang and H. J. Sung, Wall-attached structures of velocity fluctuations in a turbulent boundary layer, *Journal of Fluid Mechanics* **856**, 958 (2018).
- [8] R. Hu, X. I. A. Yang, and X. Zheng, Wall-attached and wall-detached eddies in wall-bounded turbulent flows, *Journal of Fluid Mechanics* **885**, A30 (2020).
- [9] J. H. Lee and H. J. Sung, Very-large-scale motions in a turbulent boundary layer, *J. Fluid Mech.* **673**, 80 (2011).
- [10] D. J. C. Dennis and T. B. Nickels, Experimental measurement of large-scale three-dimensional structures in a turbulent boundary layer. Part 2. Long structures, *Journal of Fluid Mechanics* **673**, 218 (2011).
- [11] R. Deshpande, D. Chandran, A. J. Smits, and I. Marusic, On the relationship between manipulated inter-scale phase and energy-efficient turbulent drag reduction, *Journal of Fluid Mechanics* **972**, A12 (2023).
- [12] N. Hutchins, T. B. Nickels, I. Marusic, and M. S. Chong, Hot-wire spatial resolution issues in wall-bounded turbulence, *Journal of Fluid Mechanics* **635**, 103 (2009).
- [13] M. Bernardini and S. Pirozzoli, Inner/outer layer interactions in turbulent boundary layers: A refined measure for the large-scale amplitude modulation mechanism, *Physics of Fluids* **23**, 061701 (2011).
- [14] I. Jacobi and B. J. McKeon, Phase relationships between large and small scales in the turbulent boundary layer, *Experiments in Fluids* **54**, 1481 (2013).
- [15] E. Dogan, R. Örlü, D. Gatti, R. Vinuesa, and P. Schlatter, Quantification of amplitude modulation in wall-bounded turbulence, *Fluid Dynamics Research* **51**, 011408 (2019).
- [16] A. Andreolli, D. Gatti, R. Vinuesa, R. Örlü, and P. Schlatter, Separating large-scale superposition and modulation in turbulent channels, *Journal of Fluid Mechanics* **958**, A37 (2023).
- [17] C. Zhang and S. I. Chernyshenko, Quasisteady quasihomogeneous description of the scale interactions in near-wall turbulence, *Physical Review Fluids* **1**, 014401 (2016).
- [18] S. Chernyshenko, Extension of qsqh theory for scale interaction in near-wall turbulence to all velocity components, *Journal of Fluid Mechanics* **916**, A52 (2021).
- [19] S. Duvvuri and B. J. McKeon, Triadic scale interactions in a turbulent boundary layer, *J. Fluid Mech.* **767**, R4 (2015).
- [20] X. I. A. Yang and M. F. Howland, Implication of Taylor's hypothesis on measuring flow modulation, *Journal of Fluid Mechanics* **836**, 222 (2018).
- [21] R. Mathis, I. Marusic, N. Hutchins, and K. R. Sreenivasan, The relationship between the velocity skewness and the amplitude modulation of the small scale by the large scale in turbulent boundary layers, *Phys. Fluids* **23**, 121702 (2011).
- [22] W. Anderson, Amplitude modulation of streamwise velocity fluctuations in the roughness sublayer: evidence from large-eddy simulations, *Journal of Fluid Mechanics* **789**, 567 (2016).
- [23] T. Kim, G. Blois, J. L. Best, and K. T. Christensen, Experimental evidence of amplitude modulation in permeable-wall turbulence, *Journal of Fluid Mechanics* **887**, A3 (2020).
- [24] Z. Harun, J. P. Monty, R. Mathis, and I. Marusic, Pressure gradient effects on the large-scale structure of turbulent boundary layers, *Journal of Fluid Mechanics* **715**, 477 (2013).
- [25] R. Deshpande, A. Van Den Bogaard, R. Vinuesa, L. Lindić, and I. Marusic, Reynolds-number effects on the outer region of adverse-pressure-gradient turbulent boundary layers, *Physical Review Fluids* **8**, 124604 (2023).
- [26] S. T. Salesky and W. Anderson, Buoyancy effects on large-scale motions in convective atmospheric boundary layers: implications for modulation of near-wall processes, *Journal of Fluid Mechanics* **856**, 135 (2018).
- [27] E. Dogan, R. E. Hanson, and B. Ganapathisubramani, Interactions of large-scale free-stream turbulence with turbulent boundary layers, *Journal of Fluid Mechanics* **802**, 79 (2016).
- [28] I. Marusic, R. Mathis, and N. Hutchins, Predictive Model for Wall-Bounded Turbulent Flow, *Science* **329**, 193 (2010).
- [29] D. T. Squire, C. Morrill-Winter, N. Hutchins, M. P. Schultz, J. C. Klewicki, and I. Marusic, Comparison of turbulent boundary layers over smooth and rough surfaces up to high Reynolds numbers, *J. Fluid Mech.* **795**, 210 (2016).
- [30] M. Abbassi, W. J. Baars, N. Hutchins, and I. Marusic, Skin-friction drag reduction in a high-Reynolds-number turbulent boundary layer via real-time control of large-scale structures, *International Journal of Heat and Fluid Flow* **67**, 30 (2017).
- [31] R. Pozuelo, Q. Li, P. Schlatter, and R. Vinuesa, An adverse-pressure-gradient turbulent boundary layer with nearly constant up to, *Journal of Fluid Mechanics* **939**, A34 (2022).
- [32] R. Vinuesa, P. S. Negi, M. Atzori, A. Hanifi, D. S. Henningson, and P. Schlatter, Turbulent boundary layers around wing sections up to $Re_c=1,000,000$, *International Journal of Heat and Fluid Flow* **72**, 86 (2018).
- [33] M. Li, W. J. Baars, I. Marusic, and N. Hutchins, Quantifying inner-outer interactions in noncanonical wall-bounded flows, *Physical Review Fluids* **8**, 084602 (2023).
- [34] R. Deshpande, A. Zampiron, D. Chandran, A. J. Smits, and I. Marusic, Near-Wall Flow Statistics in High- Re_τ Drag-Reduced Turbulent Boundary Layers, *Flow, Turbulence and Combustion* **111**, 1 (2023).
- [35] S. F. Tardu, Active control of near-wall turbulence by local oscillating blowing, *Journal of Fluid Mechanics* **439**, 217 (2001).
- [36] S. Pal, S. Deutsch, and C. Merkle, A comparison of shear stress fluctuation statistics between microbubble modified and polymer modified turbulent boundary layers, *Physics of Fluids A: Fluid Dynamics* **1**, 1360 (1989).
- [37] S. Duvvuri and B. McKeon, Nonlinear interactions isolated through scale synthesis in experimental wall turbulence, *Physical Review Fluids* **1**, 032401 (2016).
- [38] R. Deshpande, J. P. Monty, and I. Marusic, Streamwise inclination angle of large wall-attached structures in turbulent boundary layers, *Journal of Fluid Mechanics* **877**, R4 (2019).
- [39] G. Cui and I. Jacobi, Variability of convection velocities and structure inclination angles in wall-bounded turbulence, *Journal of Fluid Mechanics* **989**, A16 (2024).